RESEARCH ARTICLE | NOVEMBER 08 2021

# Local stress tensor calculation by the method-of-plane in microscopic systems with macroscopic flow: A formulation based on the velocity distribution function

Hiroki Kusudo ; Takeshi Omori ; Yasutaka Yamaguchi



*J. Chem. Phys.* 155, 184103 (2021)
https://doi.org/10.1063/5.0062889
CHORUS

The Journal of Chemical Physics ARTICLE scitation.org/journal/jcp

# Local stress tensor calculation by the method-of-plane in microscopic systems with macroscopic flow: A formulation based on the velocity distribution function

Cite as: J. Chem. Phys. 155, 184103 (2021); doi: 10.1063/5.0062889
Submitted: 9 July 2021 • Accepted: 19 October 2021 •
Published Online: 8 November 2021



Hiroki Kusudo,[1,a)] Takeshi Omori,[2,b)] and Yasutaka Yamaguchi[1,3,c)]

## AFFILIATIONS

[1] Department of Mechanical Engineering, Osaka University, 2-1 Yamadaoka, Suita 565-0871, Japan
[2] Department of Mechanical Engineering, Osaka City University, 3-3-138 Sugimoto, Sumiyoshi-ku, Osaka 558-8585, Japan
[3] Water Frontier Research Center (WaTUS), Research Institute for Science and Technology, Tokyo University of Science, 1-3 Kagurazaka, Shinjuku-ku, Tokyo 162-8601, Japan

[a)] **Author to whom correspondence should be addressed:** hiroki@nnfm.mech.eng.osaka-u.ac.jp
[b)] **Electronic mail:** omori@osaka-cu.ac.jp
[c)] **Electronic mail:** yamaguchi@mech.eng.osaka-u.ac.jp



## ABSTRACT

In this work, we developed a calculation method of local stress tensor applicable to non-equilibrium molecular dynamics (NEMD) systems, which evaluates the macroscopic momentum advection and the kinetic term of the stress in the framework of the Method-of-Plane (MoP), in a consistent way to guarantee the mass and momentum conservation. From the relation between the macroscopic velocity distribution function and the microscopic molecular passage across a fixed control plane, we derived a method to calculate the basic properties of the macroscopic momentum conservation law including the density, the velocity, the momentum flux, and the two terms of the stress tensor, i.e., the interaction and the kinetic terms, defined on a surface with a finite area. Any component of the streaming velocity can be obtained on a control surface, which enables the separation of the kinetic momentum flux into the advection and stress terms in the framework of MoP, and this enables strict satisfaction of the mass and momentum conservation for an arbitrary closed control volume (CV) set in NEMD systems. We validated the present method through the extraction of the density, velocity, and stress distributions in a quasi-one-dimensional steady-state Couette flow system and in a quasi-2D steady-state NEMD system with a moving contact line. We showed that with the present MoP, in contrast to the volume average method, the conservation law was satisfied even for a CV set around the moving contact line, which was located in a strongly inhomogeneous region.



## I. INTRODUCTION

With the increasing interest in microfluidic devices and nanotechnologies, molecular dynamics (MD) simulations have become a powerful computational tool to examine the fluid behavior for small scale systems. In addition to the static properties of the fluids and interfaces, analysis of systems with a non-zero local flow, i.e., macroscopically dynamic non-equilibrium MD (NEMD) is one of the topics of interest of a recent computational approach, which directly deals with complex nanoscale flows including the contact-line motion of simple Lennard-Jones (LJ) liquids[1–4] and more realistic ones including water.[5] For the understanding in terms of flow fields, the microscopic motion of individual molecules must be averaged, and the stress tensor plays a key role in such a macroscopic flow. Within the framework of fluid mechanics, the stress tensor is determined from the velocity fields through the constitutive

equation typically including the viscosity, and the local acceleration of the fluid is given by the gradient of the stress tensor and the external field to satisfy the momentum conservation. On the other hand, the molecular motion is governed by the intermolecular interaction, and the stress tensor is defined through the average of the molecular motion and interaction. With this respect, the microscopic stress tensor is comprised of the kinetic term and the intermolecular interaction (or configuration) term. The main scope of this article is the proper description of the kinetic term of the stress in NEMD systems.

Before the establishment of the MD method, Irving and Kirkwood[6] (IK) put forward the connection between the macroscopic conservation laws (for details, see Appendix A) and microscopic molecular motion governed by the intermolecular interaction through the statistical mechanical theory based on the distribution function in the phase space and derived an expression of the local pointwise stress comprised of kinetic and interaction parts including Taylor series expansion of differences in delta functions to express the microscopic particle feature.

After the introduction of numerical MD simulations,[7,8] the calculation of average stress in homogeneous bulk systems was enabled based on the virial theorem, which, indeed, corresponds to the average of the IK form integrated in space and time.[9,10] Regarding the local stress implemented for equilibrium MD (EMD) simulations with a discrete time step, a pragmatic scheme to calculate the averaged stress defined on a flat plane in quasi-one-dimensional (1D) planar systems[11] and a spherical curved surface[12] was proposed, where all the momentum flux and intermolecular force across the plane or the sphere, which divide the computational domain, were summed up during the time integration in macroscopically static systems. This type of stress definition is usually called the Method-of-Plane (MoP),[13–15] or Hardy[16] stress, where the momentum conservation law with the above-mentioned MoP for quasi-1D EMD systems was proved to be an exact consequence of Newton's laws for any control volume (CV) surrounded by an enclosing surface(s) irrespective of whether the local system in the CV is homogeneous or not. In addition, this momentum conservation is not restricted to quasi-1D EMD systems but also applicable to quasi-2D EMD systems, e.g., the present authors adopted the MoP for a CV with a rectangular enclosing surface set around the contact line of an equilibrium droplet to examine the nanoscale wetting behavior through the mechanical balance exerted on the fluid in the CV.[17] Another conventional approach to give local mean stress in space is the volume average (VA) method, where the weighted average of the pair interaction in local CVs is included in the formulation.[18–26] Regarding the analysis based on the macroscopic momentum conservation, which describes that the total momentum in the CV can be changed by the momentum flux, i.e., the advection and stress terms, passing the surface enclosing the CV, the VA should, in principle, be applied only for homogeneous regions because the flux on the CV boundary without thickness cannot be calculated within its framework, while stress integral can also be obtained by the VA, and this enables the calculation of the surface tension.[10,19,25,27–30] The momentum conservation is satisfied for the whole system if the VA is properly summed up; however, special care is needed to consider the momentum conservation for local CVs because the VA originally was not designed to examine local momentum conservation to be satisfied for an arbitrary CV.[16,21,26] This feature is similar to the atomic stress,[31] for instance, provided as the *stress/atom* command in LAMMPS package,[32] often used to simply visualize the stress field (see Appendix C).

In NEMD systems with a non-zero local flow with the macroscopic velocity $\boldsymbol{u} \neq \boldsymbol{0}$, local $\boldsymbol{u}$ must be defined on a surface $S$ enclosing a control volume $V$ in NEMD systems so that the stress is consistent with the macroscopic momentum conservation. In other words, if one wants to examine the macroscopic mass and momentum balances with setting an arbitrary CV in a complex flow system, e.g., a CV set around a contact line, local macroscopic properties must be defined on a finite-sized area on a CV.

In this paper, we show a calculation method of the MoP-based local stress tensor applicable to NEMD systems with a proper definition of the density and macroscopic velocity consistent with the mass and momentum conservation. We provide the formulation for systems consisting of single-component mono-atomic fluid molecules for simplicity, while the present framework is also applicable to systems of multi-component or poly-atomic fluid molecules, in which the intra-molecular interaction term (for details, see Appendix B) gives rise to a difficulty for the stress definition and resulting flux,[33] not the kinetic term in Eq. (2) discussed in the present study. Related to this point, the non-uniqueness problem of the local stress/pressure tensor due to the inhomogeneity of the liquids typically at the interface[34–39] is also an issue regarding the interaction term. For the derivation, we introduced the velocity distribution function (VDF) to give the average of physical properties defined on a fixed control plane. To check its validity, we performed test calculation in two systems: (1) a quasi-1D Couette flow system and (2) a quasi-2D system with liquid–solid–vapor contact lines, both consisted of a LJ fluid between parallel solid walls moving in the opposite directions tangential to the wall surfaces. In the first system, we compared the density and velocity distributions obtained by the present method and the VA, and we calculated the distributions of the stress components and advection term. Furthermore, we showed that the same velocity distribution was obtained on bin faces with different normal directions, which is essential to determine the advection term. In the second system, the density, velocity, and stress distributions are calculated in the complex flow with liquid–vapor interfaces and contact lines. In addition, we compared the present MoP and VA regarding the mass conservation for a CV surrounding the contact line.

## II. THEORY

We show the derivation of the kinetic term of the stress averaged on a finite bin face in a Cartesian coordinate system for a single-component mono-atomic fluid in the following for simplicity. The fluid stress tensor component $\tau_{kl}$, which expresses the stress in the $l$ direction exerted on a surface element with an outward normal in the $k$ direction, is given by the kinetic term $\tau_{kl}^{\mathrm{kin}}$ and the intermolecular interaction term $\tau_{kl}^{\mathrm{int}}$ as

$$\tau_{kl} = \tau_{kl}^{\mathrm{kin}} + \tau_{kl}^{\mathrm{int}}. \tag{1}$$

In the standard MoP for equilibrium MD systems without a mean flow consisting of single-component mono-atomic fluid molecules,[13–15,17] the kinetic term $\tau_{kl}^{\mathrm{kin}}$ in Eq. (1) on a bin face of area

$S_k$ with its normal vector pointing to the $k$th Cartesian direction is calculated by

$$\tau_{kl}^{\mathrm{kin}} \equiv -\frac{1}{S_k \delta t}\left\langle \sum_{i\in \mathrm{fluid},\delta t}^{\mathrm{crossing}\, S_k} m^i v_l^i \frac{v_k^i}{|v_k^i|} \right\rangle, \tag{2}$$

where $m^i$ and $v_l^i$ denote the mass and $l$-component of the velocity vector $\boldsymbol{v}^i$ of fluid particle $i$, respectively. We also denote the bin face by $S_k$, hereafter. The angular brackets denote the ensemble average, and the summation $\sum_{i\in \mathrm{fluid},\delta t}^{\mathrm{crossing}\, S_k}$ is taken for every fluid particle $i$ passing through $S_k$ within a time interval of $\delta t$, which is equal to the time increment for the numerical integration. Considering that we deal with single-component fluid molecules of an identical mass $m$, we substitute $m^i$ with $m$, hereafter. A sign function $\frac{v_k^i}{|v_k^i|}$ equal to $\pm 1$ is multiplied with the momentum transfer $mv_l^i$ across $S_k$ to evaluate the kinetic effect on the stress depending on the passing direction. Note that in static equilibrium systems, i.e., systems without a macroscopic local mean flow, the advection term is zero in the whole system. The definition of the interaction term of the MoP $\tau_{kl}^{\mathrm{int}}$, which is not the main scope of this article, is shown in Appendix B. Note that technically, the fluid–solid interaction can also be included in stress, but only the fluid–fluid interaction was taken into account as the fluid stress, and fluid–solid contribution was considered as an external force field.[17,40,41] In addition, note that for multi-component systems or systems with poly-atomic molecules, difficulties mainly arise to treat the interaction force between different kinds of molecules or the constraint force[42] of the poly-atomic molecules, where the interaction forces should be properly implemented into the stress calculation to satisfy the conservation laws.[33]

To extend the standard MoP to NEMD systems with a non-zero macroscopic mean local flow, the streaming velocity should be properly subtracted from the kinetic term $\tau_{kl}^{\mathrm{kin}}$ in Eq. (2) so that the macroscopic momentum flux as the advection term due to the mean velocity $\boldsymbol{u}$ may be included not in the stress term but in the advection term within the macroscopic description of the momentum conservation, i.e., in the Navier–Stokes equation. In the following, we provide a general framework to connect a microscopic variable $\xi^i$ of particles and a macroscopic field value $\xi(\boldsymbol{x},t)$ averaged on $S_k$ under non-zero mean velocity based on the local VDF in the Cartesian $xyz$ coordinate system.

At first, we define the VDF $f(\boldsymbol{x},\boldsymbol{v},t)$ for the mass with a velocity $\boldsymbol{v} = (v_x, v_y, v_z)$ at position $\boldsymbol{x} = (x, y, z)$ at time $t$, which gives the local density $\rho(\boldsymbol{x},t)$ by

$$\begin{aligned}\rho(\boldsymbol{x},t) &= \int_{-\infty}^{\infty} \mathrm{d}v_x \int_{-\infty}^{\infty} \mathrm{d}v_y \int_{-\infty}^{\infty} \mathrm{d}v_z f(\boldsymbol{x},\boldsymbol{v},t) \\ &\equiv \iiint_{-\infty}^{\infty} \mathrm{d}\boldsymbol{v} f(\boldsymbol{x},\boldsymbol{v},t),\end{aligned} \tag{3}$$

where we rewrite $\int_{-\infty}^{\infty}\mathrm{d}v_x\int_{-\infty}^{\infty}\mathrm{d}v_y\int_{-\infty}^{\infty}\mathrm{d}v_z$ as $\iiint_{-\infty}^{\infty}\mathrm{d}\boldsymbol{v}$. Then, a microscopic variable $\xi^i$ per mass of particle $i$ can be related to the corresponding macroscopic field variable $\xi(\boldsymbol{x},t)$ as

$$\lim_{\delta t\to 0}\left\langle \sum_{i\in \mathrm{fluid},\delta t}^{\mathrm{crossing}\, S_k} m\xi^i \right\rangle \equiv \lim_{\delta t\to 0} \iiint_{-\infty}^{\infty} \mathrm{d}\boldsymbol{v} \int_0^{|v_k|\delta t} \mathrm{d}x_k S_k f(\boldsymbol{x},\boldsymbol{v},t)\xi(\boldsymbol{x},t). \tag{4}$$

The RHS denotes the integral weighted with the VDF considering an oblique pillar of a base area $S_k$ and a height $|v_k|\delta t$ with its central axis parallel to $\boldsymbol{v}$, which is typically assumed upon the derivation of the equilibrium pressure in the kinetic theory of gases.

With the limit $\delta t \to 0$ and by rewriting the average of $f(\boldsymbol{x},\boldsymbol{v},t)$ and $\xi(\boldsymbol{x},t)$ in the oblique pillar by $f(S_k,\boldsymbol{v},t)$ and $\xi(S_k,t)$, respectively, the integral with respect to $x_k$ in the RHS of Eq. (4) writes

$$\lim_{\delta t\to 0}\int_0^{|v_k|\delta t} \mathrm{d}x_k S_k f(\boldsymbol{x},\boldsymbol{v},t)\xi(\boldsymbol{x},t) = \lim_{\delta t\to 0} S_k f(S_k,\boldsymbol{v},t)\xi(S_k,t)|v_k|\delta t, \tag{5}$$

and it follows for Eq. (4) that

$$\lim_{\delta t\to 0}\left\langle \sum_{i\in \mathrm{fluid},\delta t}^{\mathrm{crossing}\, S_k} m\xi^i \right\rangle = \lim_{\delta t\to 0} S_k \iiint_{-\infty}^{\infty} \mathrm{d}\boldsymbol{v} f(S_k,\boldsymbol{v},t)\xi(S_k,t)|v_k|\delta t. \tag{6}$$

Hence, by dividing both sides by $S_k\delta t$,

$$\iiint_{-\infty}^{\infty} \mathrm{d}\boldsymbol{v} f(S_k,\boldsymbol{v},t)\xi(S_k,t)|v_k| = \lim_{\delta t\to 0}\frac{1}{S_k\delta t}\left\langle \sum_{i\in \mathrm{fluid},\delta t}^{\mathrm{crossing}\, S_k} m\xi^i \right\rangle \tag{7}$$

is derived as a basic equation for the connection between the macroscopic field variable $\xi(S_k,t)$ and microscopic variable $\xi^i$, which belongs to the constituent particle $i$ upon crossing $S_k$.

Now, we proceed to the expressions of the macroscopic field variables averaged on $S_k$. By substituting $\xi(S_k,t)$ and $\xi^i$ in Eq. (7) with $\frac{1}{|v_k|}$ and $\frac{1}{|v_k^i|}$, respectively, and using Eq. (3), we obtain

$$\rho(S_k,t) = \lim_{\delta t\to 0}\frac{1}{S_k\delta t}\left\langle \sum_{i\in \mathrm{fluid},\delta t}^{\mathrm{crossing}\, S_k} \frac{m}{|v_k^i|} \right\rangle, \tag{8}$$

where $v_k^i$ denotes the velocity component in the $k$ direction of particle $i$. Similarly, regarding the macroscopic mass flux $\rho u_l$ given by

$$\rho u_l(\boldsymbol{x},t) = \iiint_{-\infty}^{\infty} \mathrm{d}\boldsymbol{v} f(\boldsymbol{x},\boldsymbol{v},t) v_l, \tag{9}$$

substituting $\xi(S_k,t)$ and $\xi^i$ in Eq. (7) with $\frac{v_l}{|v_k|}$ and $\frac{v_l^i}{|v_k^i|}$, respectively, leads to

$$\rho u_l(S_k,t) = \lim_{\delta t\to 0}\frac{1}{S_k\delta t}\left\langle \sum_{i\in \mathrm{fluid},\delta t}^{\mathrm{crossing}\, S_k} \frac{mv_l^i}{|v_k^i|} \right\rangle. \tag{10}$$

From Eqs. (8) and (10), the macroscopic velocity $u_l$ results in

$$u_l(S_k,t) = \frac{\rho u_l(S_k,t)}{\rho(S_k,t)} = \lim_{\delta t\to 0}\frac{\left\langle \sum_{i\in \mathrm{fluid},\delta t}^{\mathrm{crossing}\, S_k} \frac{mv_l^i}{|v_k^i|} \right\rangle}{\left\langle \sum_{i\in \mathrm{fluid},\delta t}^{\mathrm{crossing}\, S_k} \frac{m}{|v_k^i|} \right\rangle}. \tag{11}$$

Finally, to write the kinetic contribution of the stress $\tau_{kl}^{\mathrm{kin}}$, we use the expression in the kinetic theory of gases given by

$$\tau_{kl}^{\mathrm{kin}}(\boldsymbol{x},t) = -\iiint_{-\infty}^{\infty} \mathrm{d}\boldsymbol{v} f(\boldsymbol{x},\boldsymbol{v},t)(v_k - u_k(\boldsymbol{x},t))(v_l - u_l(\boldsymbol{x},t)). \tag{12}$$

By expanding Eq. (12), we obtain

$$\begin{aligned}\tau_{kl}^{\mathrm{kin}}(\boldsymbol{x},t) &= -\iiint_{-\infty}^{\infty} \mathrm{d}\boldsymbol{v} f(\boldsymbol{x},\boldsymbol{v},t) v_k (v_l - u_l(\boldsymbol{x},t)) \\ &\quad + u_k(\boldsymbol{x},t) \iiint_{-\infty}^{\infty} \mathrm{d}\boldsymbol{v} f(\boldsymbol{x},\boldsymbol{v},t)(v_l - u_l(\boldsymbol{x},t)) \\ &= -\iiint_{-\infty}^{\infty} \mathrm{d}\boldsymbol{v} f(\boldsymbol{x},\boldsymbol{v},t) v_k (v_l - u_l(\boldsymbol{x},t)) + u_k \rho u_l(\boldsymbol{x},t) \\ &\quad - u_k \rho u_l(\boldsymbol{x},t) \\ &= -\iiint_{-\infty}^{\infty} \mathrm{d}\boldsymbol{v} f(\boldsymbol{x},\boldsymbol{v},t) v_k (v_l - u_l(\boldsymbol{x},t)). \end{aligned} \tag{13}$$

Hence, by substituting $\xi(S_k,t)$ and $\xi^i$ in Eq. (7) with $-\frac{v_k(v_l-u_l)}{|v_k|}$ and $-\frac{v_k^i(v_l^i-u_l)}{|v_k^i|}$, respectively, we obtain

$$\begin{aligned}\tau_{kl}^{\mathrm{kin}}(S_k,t) &= \lim_{\delta t\to 0}\left[-\frac{1}{S_k \delta t}\left\langle \sum_{i\in \mathrm{fluid},\delta t}^{\mathrm{crossing}\, S_k} \frac{m v_k^i (v_l^i - u_l(S_k,t))}{|v_k^i|}\right\rangle\right] \\ &= \lim_{\delta t\to 0}\left(-\frac{1}{S_k \delta t}\left\langle \sum_{i\in \mathrm{fluid},\delta t}^{\mathrm{crossing}\, S_k} \frac{m v_k^i v_l^i}{|v_k^i|}\right\rangle \right. \\ &\quad \left. + u_l(S_k,t)\frac{1}{S_k\delta t}\left\langle \sum_{i\in \mathrm{fluid},\delta t}^{\mathrm{crossing}\, S_k} \frac{m v_k^i}{|v_k^i|}\right\rangle\right) \\ &= -\lim_{\delta t\to 0}\frac{1}{S_k\delta t}\left\langle \sum_{i\in \mathrm{fluid},\delta t}^{\mathrm{crossing}\, S_k} \frac{m v_k^i v_l^i}{|v_k^i|}\right\rangle + \rho u_l u_k(S_k,t), \end{aligned} \tag{14}$$

where Eq. (10) is used in the final equality. Note that the second term in the rightmost-HS can be obtained by

$$\rho u_l u_k(S_k,t) = \frac{\rho u_l(S_k,t)\cdot \rho u_k(S_k,t)}{\rho(S_k,t)} \tag{15}$$

using Eqs. (10) and (11), which correspond to the advection term in the macroscopic momentum conservation in the Navier–Stokes equation (for details, see Appendix A). By subtracting $\rho u_l u_k(S_k,t)$ from the rightmost-HS and leftmost-HS of Eq. (14), we obtain

$$\tau_{kl}^{\mathrm{kin}}(S_k,t) - \rho u_l u_k(S_k,t) = -\lim_{\delta t\to 0}\frac{1}{S_k\delta t}\left\langle \sum_{i\in \mathrm{fluid},\delta t}^{\mathrm{crossing}\, S_k} \frac{m v_k^i v_l^i}{|v_k^i|}\right\rangle, \tag{16}$$

meaning that the microscopic total momentum transfer in the RHS corresponds to the stress minus the advection term in the LHS. Technically, the summation in the RHS of Eq. (16) is calculated during the MD simulation, and as the post-process, the stress $\tau_{kl}^{\mathrm{kin}}(S_k,t)$ is obtained by adding the advection term $\rho u_l u_k$ to the total microscopic momentum transfer as

$$\tau_{kl}^{\mathrm{kin}}(S_k,t) = \left[\tau_{kl}^{\mathrm{kin}}(S_k,t) - \rho u_l u_k(S_k,t)\right] + \rho u_l u_k(S_k,t), \tag{17}$$

where the advection term is calculated by dividing $\rho u_l(S_k,t)\cdot \rho u_k(S_k,t)$ by the density $\rho(S_k,t)$ as in Eq. (15): all obtained as the post-process.

The relations between the macroscopic variables in the mass and momentum conservations and microscopic expressions are summarized in Table I.

In practice, within the framework of MD, $\delta t(\to 0)$ must be replaced by a small non-zero time step of $\Delta t$ for numerical integration. Upon this procedure without this limit, we have to assume the following: (1) the change in the distribution function $f(\boldsymbol{x},\boldsymbol{v},t)$ within the distance range of $|\boldsymbol{v}|\delta t$ is negligibly small and (2) the values of $v_k^i$ and $v_l^i$ upon "crossing" should be properly evaluated based on the position update procedure of particles depending on the time integration scheme. For the velocity Verlet method, which is applied in the numerical test in Sec. III, we adopted $\boldsymbol{v}^i \equiv \frac{\boldsymbol{x}^i(t+\Delta t)-\boldsymbol{x}^i(t)}{\Delta t}$ using the positions $\boldsymbol{x}^i(t)$ and $\boldsymbol{x}^i(t+\Delta t)$ of fluid particle $i$ at times $t$ and $t+\Delta t$ before and after crossing the bin face to avoid the discrepancy in the mass flux by the MoP calculation and by the position update.

Note that Eq. (16) without the limit $\delta t \to 0$ is the same as the RHS of Eq. (2), which simply sums up the momentum

**TABLE I.** Microscopic expressions for the calculation of the corresponding macroscopic properties defined as the average on the bin face $S_k$ in NEMD systems. The top four properties can be directly calculated from NEMD systems through the MoP procedure, whereas the others below are derived from the four.

| Macroscopic property | Microscopic expression | Corresponding equation(s) |
|---|---|---|
| $\rho(S_k,t)$ | $\lim_{\delta t\to 0}\frac{1}{S_k\delta t}\left\langle \sum_{i\in \mathrm{fluid},\delta t}^{\mathrm{crossing}\, S_k} \frac{m}{\lvert v_k^i\rvert}\right\rangle$ | Eq. (8) |
| $\rho u_l(S_k,t)$ | $\lim_{\delta t\to 0}\frac{1}{S_k\delta t}\left\langle \sum_{i\in \mathrm{fluid},\delta t}^{\mathrm{crossing}\, S_k} \frac{m v_l^i}{\lvert v_k^i\rvert}\right\rangle$ | Eq. (10) |
| $\tau_{kl}^{\mathrm{int}}(S_k,t)$ | $-\frac{1}{S_k}\left\langle \sum_{(i,j)\in \mathrm{fluid}}^{\mathrm{across}\, S_k} F_l^{ij}\frac{r_k^{ij}}{\lvert r_k^{ij}\rvert}\right\rangle$ | Eq. (B1) |
| $\tau_{kl}^{\mathrm{kin}}(S_k,t) - \rho u_l u_k(S_k,t)$ | $-\lim_{\delta t\to 0}\frac{1}{S_k\delta t}\left\langle \sum_{i\in \mathrm{fluid},\delta t}^{\mathrm{crossing}\, S_k} \frac{m v_k^i v_l^i}{\lvert v_k^i\rvert}\right\rangle$ | Eq. (16) |
| $u_l = \frac{\rho u_l}{\rho}$ | ⋯ | Eq. (11) |
| $\rho u_l u_k$ | ⋯ | Eq. (15) |
| $\tau_{kl}^{\mathrm{kin}} = \left(\tau_{kl}^{\mathrm{kin}} - \rho u_l u_k\right) + \rho u_l u_k$ | ⋯ | Eq. (17) |
| $\tau_{kl} = \tau_{kl}^{\mathrm{kin}} + \tau_{kl}^{\mathrm{int}}$ | ⋯ | Eq. (1) |

transfer across the bin face $S_k$ with a sign function $\frac{v_k^i}{|v_k^i|}$. Hence, if one locates a CV with a closed surface consisting of the MoP bin faces, then the momentum conservation is strictly satisfied with Eq. (16). Different choices are, indeed, possible to determine the advection term $\rho u_l u_k(S_k,t)$ in Eq. (15) to separate the stress $\tau_{kl}^{\mathrm{kin}}(S_k,t)$ from $\tau_{kl}^{\mathrm{kin}}(S_k,t) - \rho u_l u_k(S_k,t)$ by Eq. (17), and this may sound that the definition of $\tau_{kl}^{\mathrm{kin}}(S_k,t)$ is not unique. However, by setting $l = k$ in Eq. (10), the surface normal mass flux is evaluated as the simple sum of the mass passage with a sign function $\frac{v_k^i}{|v_k^i|}$, and this strictly satisfies the mass conservation, meaning that one can choose a unique definition of $\rho u_l u_k(S_k,t)$ that simultaneously satisfies the macroscopic mass and momentum conservation.

Another point to be noted is that the final forms in Eqs. (8), (10), and (16) are formally equivalent to the MoP expressions by Daivis, Travis, and Todd,[43] which were derived for a quasi-one-dimensional flow through the expressions of the time derivative of the fluxes in a CV with the Fourier transform and were, in principle, applicable for the average on an infinite plane under a periodic boundary condition. On the other hand, our non-flux-based derivation with a definition of physical properties averaged on a face through the VDF enables the calculation of physical properties on a finite area. In addition, taking advantage of this non-flux-based feature, one can calculate, for instance, the velocity component $u_l$ on a bin face $S_k (l \neq k)$ tangential to the velocity component by Eq. (11). This point will be discussed more in detail with a quasi-1D Couette-type flow in Sec. III A as an example.

## III. NUMERICAL TEST

The extended MoP was tested through the calculation of the density, macroscopic mean velocity, and stress distributions in two systems with a Lennard-Jones (LJ) fluid: a quasi-1D Couette-type flow and a quasi-2D shear flow with solid–liquid–vapor contact lines. Note that both the systems are in steady state, and we applied time average instead of ensemble average.

### A. Quasi-1D Couette-type flow

Figure 1(a) shows the MD simulation system of a quasi-1D Couette-type flow, where the basic setup is a standard one similar to our previous study.[44,45] The two parallel solid walls were fcc crystals, and every pair of the nearest neighbors in the walls was bound through a harmonic potential $\Phi_{\mathrm{h}}(r) = \frac{k}{2}(r - r_{\mathrm{eq}})^2$, with $r$ being the interparticle distance, $r_{\mathrm{eq}} = 0.277$ nm, and $k = 46.8$ N/m. Interactions between fluid particles and between fluid and solid particles were modeled by a 12-6 LJ potential $\Phi^{\mathrm{LJ}}(r_{ij}) = 4\epsilon_{ij}\left[\left(\frac{\sigma_{ij}}{r_{ij}}\right)^{12} - \left(\frac{\sigma_{ij}}{r_{ij}}\right)^{6}\right]$, where $r_{ij}$ is the distance between the particles $i$ and $j$, while $\epsilon$ and $\sigma$ denoted the LJ energy and length parameters, respectively. This LJ interaction was truncated at a cutoff distance of $r_{\mathrm{c}} = 3.5\sigma$, and quadratic functions were added so that the potential and interaction forces smoothly vanished at $r_{\mathrm{c}}$.[29] We used the following parameters for fluid–fluid (ff) and solid–fluid (sf) interactions: $\sigma_{\mathrm{ff}} = 0.340$ nm, $\epsilon_{\mathrm{ff}} = 1.67 \times 10^{-21}$ J, $\sigma_{\mathrm{sf}} = 0.345$ nm, and $\epsilon_{\mathrm{sf}} = 0.646 \times 10^{-21}$ J. The atomic masses of fluid and solid particles were $m_{\mathrm{f}} = 39.95$ u and $m_{\mathrm{s}} = 195.1$ u, respectively. Finally, the equations of motion were

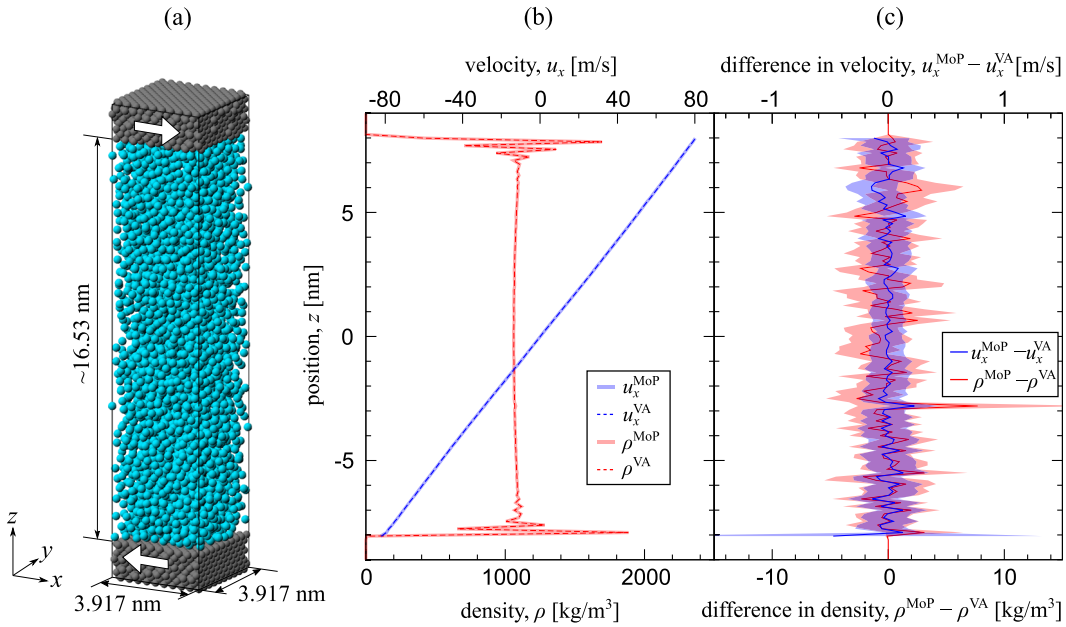


**FIG. 1.** (a) Quasi-1D Couette-type flow system of a Lennard-Jones liquid confined between two solid walls. (b) Distributions of density $\rho$ and velocity $u_x$ calculated by the proposed Method-of-Plane (MoP) and the volume average (VA). Solid and dashed lines denote the results of MoP and VA, respectively, while the two lines almost overlap in this scale. (c) Difference between the MoP and the VA regarding density $\rho^{\mathrm{MoP}} - \rho^{\mathrm{VA}}$ and velocity $u_x^{\mathrm{MoP}} - u_x^{\mathrm{VA}}$ with their error bars depicted with semi-transparent areas around the average.

integrated using the velocity Verlet algorithm, with a time step $\Delta t$ of 5 fs.

The periodic boundary condition was set in the $x$ and $y$ directions, and 4000 LJ particles were confined between two parallel solid walls consisting of the fcc crystal located on the bottom and top sides of the calculation cell, which directed (001) and $(00\bar{1})$ planes normal to the $z$ direction. Both had eight layers so that the possible minimum distance between the fluid particle and the solid particle in the outmost layer was longer than the cutoff distance. The relative positions of the solid particles in the outmost layers of each base crystal were fixed, and the temperature of those in the second outermost layers was controlled at a control temperature of 100 K by using the standard Langevin thermostat.[46] The system was first equilibrated for 10 ns using the top wall as a piston with a control pressure of 4 MPa without shear so that a quasi-1D system with a LJ liquid confined between fcc solid walls was achieved. After the equilibration, a further relaxation run to achieve a steady shear flow was carried out for 10 ns by moving the particles in the outmost layers of both walls with opposite velocities of ±100 m/s in the $x$ direction, using the top wall as a piston with a control pressure of 4 MPa. Finally, steady shear flow simulation was carried out, keeping their $z$ position constant at the average position during the second relaxation run, where the system pressure resulted in 3.61 MPa.

We tested the MoP expression (Table I) in the steady state, where the local density, velocity, advection term, and stress were obtained as a time average of 200 ns on a grid with $x$-normal bin faces with a height of $\Delta z = 0.150$ nm and $z$-normal ones with a width of $\Delta x = 0.145$ nm. Assuming that the system is quasi-1D, the distribution in the $x$ direction was averaged for bins with identical $z$ positions. For comparison, we also obtained the density and velocity distributions based on a standard VA, where the time average in equally divided bin volumes parallel to the solid wall with a height of 0.150 nm was calculated.

Figure 1(b) shows the distributions of density $\rho$ and macroscopic velocity in the $x$ direction $u_x$ calculated by the proposed MoP and standard VA as a reference. Note that these distributions by the MoP can be calculated both on $x$-normal bin faces and on $z$-normal ones as shown later, while only the distributions obtained on $x$-normal bin faces are shown as the MoP results here. Overall, the MoP well reproduced the results by the VA, and the two lines almost overlap in this scale. Regarding the density distribution, except near the walls where layered structures are observed, a bulk liquid with almost constant density was formed. Note that the bulk density was not completely constant because the temperature was not constant due to the viscous heat dissipation induced by the extreme shear imposed on this system. The shear velocity profiles are linear throughout almost all the liquid part except in layered structures, which can be understood by the change in local viscosity there. The density and velocity differences between the MoP and the VA are shown in Fig. 1(c). The density difference was within 10 kg/m$^3$, which is less than 1% of the bulk density, and the velocity difference was also within 0.5 m/s, showing that the proposed MoP can extract the density and velocity distribution consistent with the VA.

Figure 2(a) shows the distributions of $\tau_{zz}(\equiv \tau_{zz}^{\mathrm{int}} + \tau_{zz}^{\mathrm{kin}})$, $\tau_{xx} - \rho u_x u_x [\equiv \tau_{xx}^{\mathrm{int}} + (\tau_{xx}^{\mathrm{kin}} - \rho u_x u_x)]$, and $\rho u_x u_x$, where the first two were directly obtained with simple addition based on Eqs. (B1) and (14) as also listed in the top part of Table I, while $\rho u_x u_x$ was obtained from the density $\rho$ and velocity $u_x$. Note that $\tau_{zz} - \rho u_z u_z$ is shown as $\tau_{zz}$ because $u_z$ is equal to zero in the whole area of the present system. In addition, note that the calculation of $\tau_{kl}^{\mathrm{int}}$ in Eq. (B1) was the same as



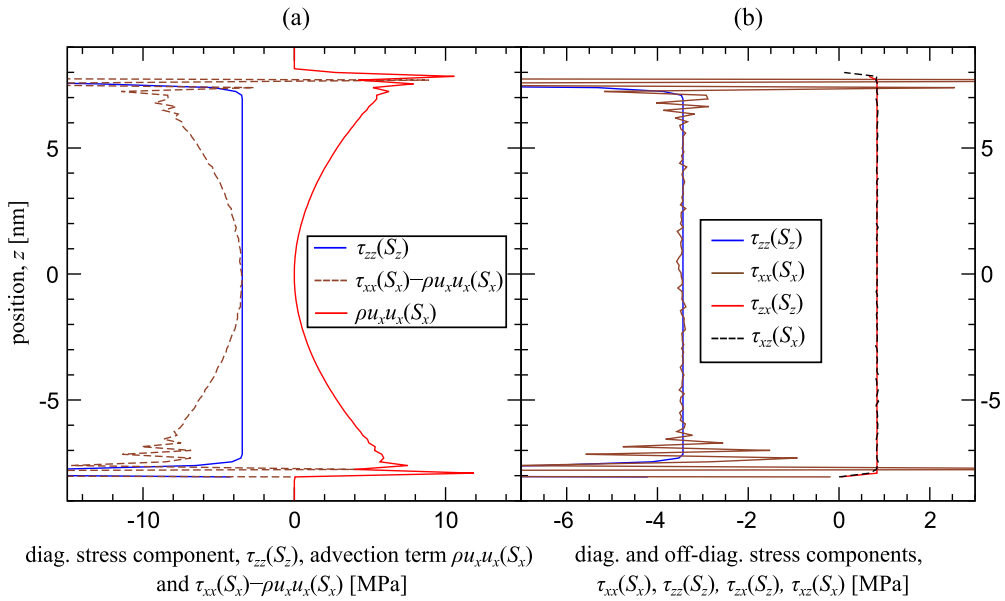


**FIG. 2.** Distributions of (a) the diagonal stress component $\tau_{zz}(S_z)(\equiv \tau_{zz}^{\mathrm{int}} + \tau_{zz}^{\mathrm{kin}})$, advection term $\rho u_x u_x(S_x)$, and $\tau_{xx}(S_x) - \rho u_x u_x(S_x)[\equiv \tau_{xx}^{\mathrm{int}} + (\tau_{xx}^{\mathrm{kin}} - \rho u_x u_x)]$, and (b) diagonal and off-diagonal stress components $\tau_{xx}(S_x)$, $\tau_{zz}(S_z)$, $\tau_{zx}(S_z)$, and $\tau_{xz}(S_x)$.

that in equilibrium systems without a macroscopic flow. As clearly observed, $\tau_{xx} - \rho u_x u_x$ including the advection and $\tau_{zz}$ are different away from the solid walls, indicating that the flow effect should be removed to properly evaluate the fluid stress. Figure 2(b) displays the distributions of the stress component $\tau_{xx}$, $\tau_{zz}$, $\tau_{zx}$, and $\tau_{xz}$, where $\tau_{zz}$ and $\tau_{zx}$ were calculated on $z$-normal bins, whereas the others were obtained on $x$-normal bins. As explained above, the stress value $\tau_{xx}$ was calculated by adding $\rho u_x u_x$ to $\tau_{xx} - \rho u_x u_x$, whereas the advection terms for the others can be neglected considering $u_z = 0$. In the bulk region sufficiently away from the walls, $\tau_{xx} = \tau_{zz}$ and $\tau_{zx} = \tau_{xz}$ are satisfied as expected from the solution of a laminar Couette flow, and the former indicates that the stress $\tau_{xx}$ is adequately calculated by the proposed MoP with the resulting value $-\tau_{xx}(= -\tau_{zz})$ equal to the external pressure value of 3.61 MPa. The wall-tangential diagonal stress $\tau_{xx}$ fluctuates near the walls as typically observed also in equilibrium systems,[17,29] because of the layered structure of the liquid as displayed in the density distribution in Fig. 1(b). On the other hand, $\tau_{zz}$ was constant except near the walls, where the solid–liquid (SL) interaction acts as the external force on the liquid. Regarding the off-diagonal components $\tau_{zx}(= \tau_{xz})$, they were constant except just around the walls, where friction from the solid is included in the force balance even in the laminar flow.

In addition to the normal velocity component $u_k$ on the MoP plane $S_k$, the calculation of $u_l(l \neq k)$ tangentially to $S_k$ is needed for the separation of $\tau_{kl}^{\mathrm{kin}}(S_k) - \rho u_l u_k(S_k)$ in Eq. (17) to properly define the stress in general flows with $u_l \neq 0$ and $u_k \neq 0$. Including this tangential velocity, we compared the distributions of the density $\rho$, the mass flux $\rho u_x$, and the velocity $u_x$ averaged on $x$-normal and $z$-normal bin faces as another numerical test in the present system in Fig. 1. More concretely, the densities $\rho(S_x)$ and $\rho(S_z)$ averaged on $x$-normal and $z$-normal bin faces $S_x$ and $S_z$, respectively, were calculated by Eq. (8) with setting $k = x$ and $k = z$, whereas the macroscopic mass fluxes $\rho u_x(S_x)$ and $\rho u_x(S_z)$ were obtained by Eq. (10) with $l = x$ on $S_x$ and $S_z$, respectively. With these definitions, $u_x(S_x) \equiv \frac{\rho u_x(S_x)}{\rho(S_x)}$ on $S_x$ and $u_x(S_z) \equiv \frac{\rho u_x(S_z)}{\rho(S_z)}$ on $S_z$ can be obtained as in Eq. (11). Note that in the present laminar flow system with $u_z = 0$, the calculation of $u_x$ is practically not needed for the stress separation of $\tau_{zz}^{\mathrm{kin}}$, $\tau_{zx}^{\mathrm{kin}}$, and $\tau_{xz}^{\mathrm{kin}}$ in Eq. (17). Figure 3 shows the distributions of the (a) density $\rho$, (b) mass flux $\rho u_x$, and (c) velocity $u_x$ defined on $x$-normal and $z$-normal bin faces in the system in Fig. 1, where the values averaged on each bin face of $x$-normal and $z$-normal are plotted with setting the $z$ position at the center of each bin face, respectively, i.e., they are staggered by $\Delta z/2$. In the bulk, $\rho$, $\rho u_x$, and resulting $u_x$ averaged on bin faces with different normal directions agreed well, indicating that the separation of the stress and advection terms in Eq. (17) is possible with the velocity values properly evaluated by the proposed method. The difference seen around the top and the bottom is due to the layered structures around the two walls, i.e., the values on $S_z$ are the average on a surface parallel to the layered structure, whereas those on $S_x$ are the average across the layers.

### B. Quasi-2D shear flow with solid–liquid–vapor contact lines

The top panel of Fig. 4 shows the MD simulation system of a quasi-2D Couette-type flow, where the basic setups are the same as



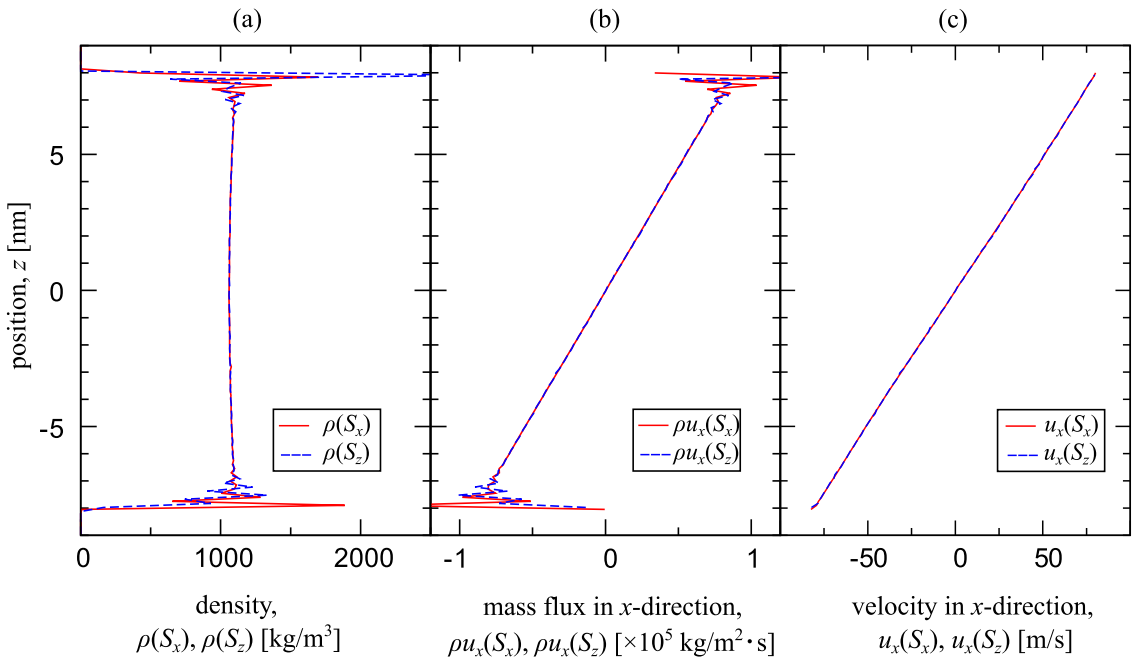


**FIG. 3.** Comparison of the time-averaged distributions of the (a) density $\rho$, (b) mass flux $\rho u_x$, and (c) velocity $u_x$ averaged on $x$-normal and $z$-normal bin faces $S_x$ and $S_z$, respectively.

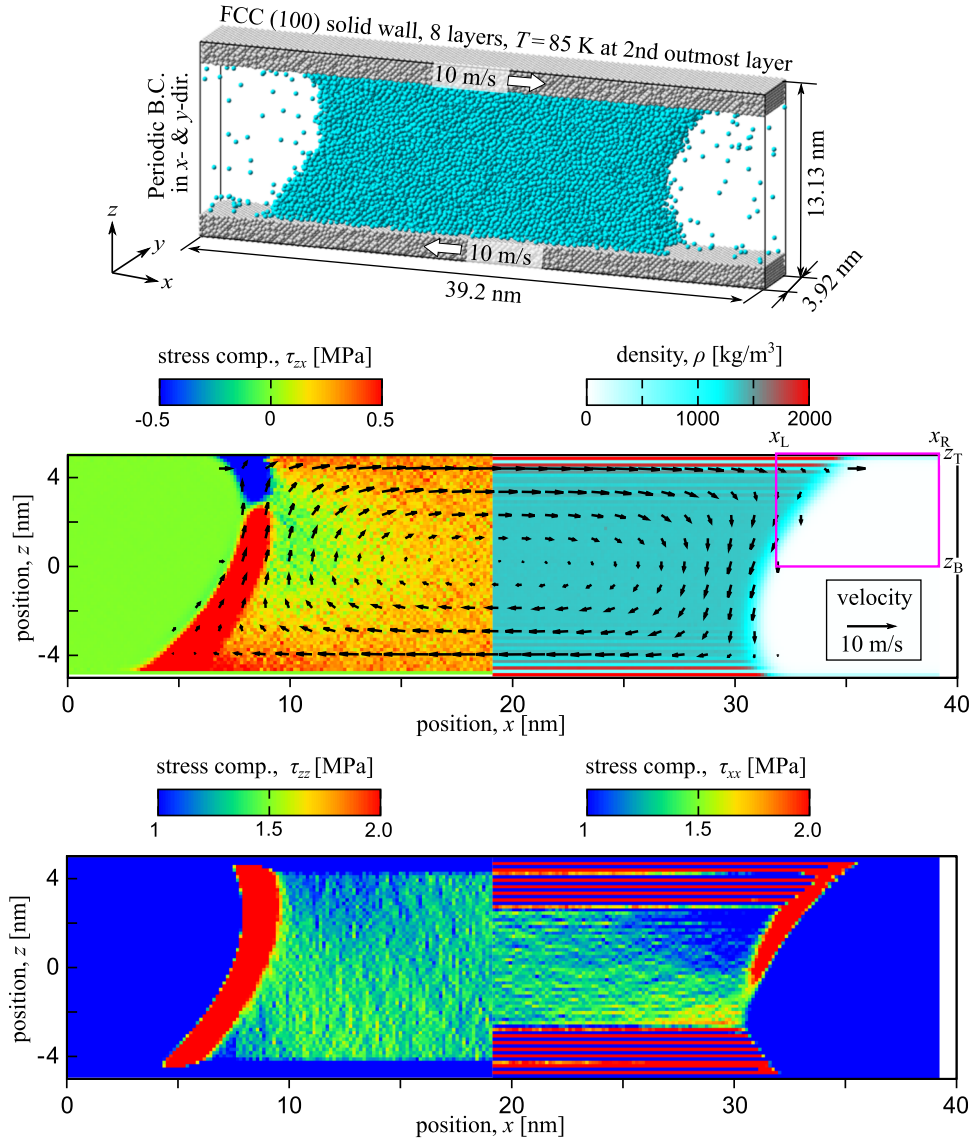


**FIG. 4.** (Top) Quasi-2D Couette-type flow system of a Lennard-Jones liquid confined between two solid walls. (Middle) Distributions of density $\rho(S_x)$, velocity $\boldsymbol{u}$, and off-diagonal stress component $\tau_{zx}(S_z)$. The black arrow denotes the macroscopic velocity calculated by the proposed Method-of-Plane. The rectangle set around the contact line shown in magenta is the control volume, for which mass conservation is checked in Table II. (Bottom) Distributions of diagonal stress components $\tau_{xx}(S_x)$ and $\tau_{zz}(S_z)$.

those in the quasi-1D system. The periodic boundary condition was set in the $x$ and $y$ directions, and 20 000 LJ particles were confined between two parallel solid walls with a distance of about 10.4 nm and a dimension of $x \times y = 39.2 \times 3.92$ nm$^2$ so that the LJ fluid may form two quasi-2D menisci with contact lines on the walls upon the preliminary equilibration at a control temperature of $T = 85$ K without shear. The static contact angles on both top and bottom walls were about 57°. After the equilibration, further relaxation runs to achieve a steady shear flow with asymmetric menisci were carried out for 10 ns by moving the particles in the outmost layers of both the walls with opposite velocities of ±10 m/s in the $x$ direction.

After the relaxation run, the density, velocity, and stress distributions were obtained by the present MoP expression in the steady state with a time average of 500 ns on $x$-normal bin faces with a length of $\Delta z = 0.149$ nm and $z$-normal ones with a length of $\Delta x = 0.150$ nm.

The middle panel of Fig. 4 shows the distributions of density $\rho(S_x)$ calculated on the $x$-normal bin faces, the velocity vector with components calculated on each bin face corresponding the component direction, and a stress component $\tau_{zx}(S_z)$ calculated on the $z$-normal bin faces, where those for $\rho(S_x)$ and $\tau_{zx}(S_z)$ are displayed only for half of the system with respect to the center of mass of

the fluid considering the symmetry. A clockwise caterpillar-like flow is clearly captured by the present method, where the shear stress $\tau_{zx}(S_z)$ distribution in the liquid phase shows the non-uniformity of the viscous stress. The strong tensile stress seen in the $\tau_{zx}(S_z)$ distribution around the liquid-vapor (LV) interfaces is due to the LV interfacial tension. The bottom panel of Fig. 4 shows the distributions of diagonal stress components $\tau_{xx}(S_x)$ and $\tau_{zz}(S_z)$. Layered structures are observed for $\tau_{xx}(S_x)$ near the SL interfaces due to the adsorption layers in the density distribution. The relation between the density layers and stress distribution near the solid walls is qualitatively the same as that in our previous study of the static droplet:[17] negative stress was seen in the adsorption layers, i.e., the adsorption layers were compressed, whereas tensile stress appeared between the layers.

Even with the VA, it is, indeed, possible to give the density and streaming velocity values on a bin face, e.g., through the interpolation of these values of adjacent bin volumes; however, to remove the advection term from the momentum transfer in Eq. (17), such formulation would cause an inconsistency with the local mass conservation for a CV when its boundary is set at a position with inhomogeneous density. To show this point, we set a rectangular CV surrounding the contact line shown in magenta in the middle panel of Fig. 4 and calculated the mass balance. The $x$-normal right and left faces are at $x_R = 39.2$ nm and $x_L = 32.3$ nm, respectively, and the $z$-normal bottom and top faces are at $z_B = 0.0$ nm and $z_T = 5.1$ nm, respectively, where $z_T$ is higher than the limit where the fluid particle can reach.[17,40,41,47] Considering that the mass flux on the top face is zero with the present setting, we calculated the mass flow rates on the left, right, and bottom faces given by

$$\dot{m}_L \equiv \int_{z_B}^{z_T} \mathrm{d}z \rho(x_L, z) u_x(x_L, z), \tag{18}$$

$$\dot{m}_R \equiv \int_{z_B}^{z_T} \mathrm{d}z \rho(x_R, z) u_x(x_R, z), \tag{19}$$

and

$$\dot{m}_B \equiv \int_{x_L}^{x_R} \mathrm{d}x \rho(x, z_B) u_z(x, z_B), \tag{20}$$

respectively, by the present MoP and VA. For the calculation with the MoP, the average density $\rho$ and velocity $\boldsymbol{u}$ defined on each bin face consisting of the CV faces are used for the numerical integration in Eqs. (18)–(20), whereas for the VA, the averages of the molecular momentum in adjacent bin volumes with $\Delta z = 0.149$ nm and $\Delta x = 0.150$ nm sandwiching the CV face, corresponding to the MoP bin face, are used as shown in Fig. 5. For the right and left CV faces, these interpolated values can be viewed as the average values for bins of $\Delta x = 0.300$ nm and $\Delta z = 0.149$ nm, and for the bottom CV face, these interpolated values can be viewed as the average values for bins of $\Delta x = 0.150$ nm and $\Delta z = 0.298$ nm. Based on the mass conservation which describes that the total mass in the CV should be changed by the mass flux (for details, see Appendix A), we compared the total mass flow rate $\dot{m}_R - \dot{m}_L - \dot{m}_B$ with the time derivative of the mass in the CV given by

$$\dot{M}_{CV} \equiv \frac{\iint_{CV} \mathrm{d}V \rho(\boldsymbol{x}, t_{end}) - \iint_{CV} \mathrm{d}V \rho(\boldsymbol{x}, t_{init})}{t_{end} - t_{init}}, \tag{21}$$

where $\iint_{CV}$ denotes the volume integral for the present CV, and the RHS was calculated by counting the difference in the number of fluid particles in the CV between the sampling interval $t_{init}$ and $t_{end}$. Note that $\dot{M}_{CV}$ is not exactly zero even under steady state because the contact line is microscopically fluctuating with time.[3,48]

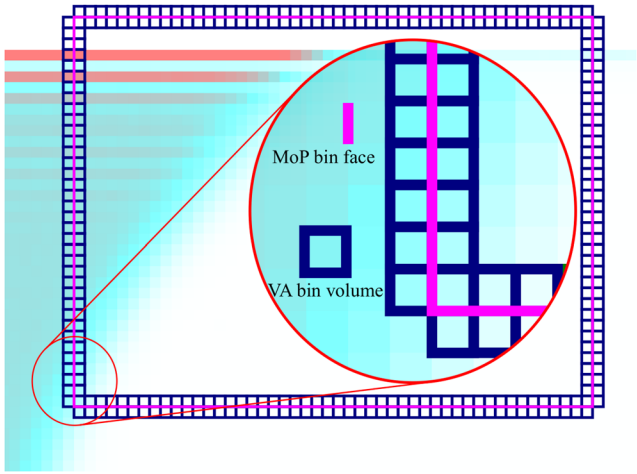


**FIG. 5.** VA bin volumes shown in dark blue around the control volume (CV) shown in magenta (identical to the CV in Fig. 4). The mass fluxes on the CV face were obtained by the interpolation of the values of adjacent VA bin volumes and compared with the mass flux calculated by the MoP on the bin face shown in magenta.

Table II shows the comparison between the MoP and VA regarding the mass flow rate across the three CV faces. Although the error bar is still large even with the average for about 500 ns, the mean time derivative in Eq. (21) is considered to be equal to the total mass flow rate with the MoP, which is in contrast to the VA that does not seem to satisfy the mass conservation for the present finite-sized VA bin volume. Specifically, this inconsistency is mainly caused on the left face of the CV where strong inhomogeneity exists due to the liquid–vapor interface, while no inconsistency is shown on the other faces set in the vapor phase of no strong inhomogeneity. Of course, this inconsistency would vanish in the limit that the size of the VA bin approaches zero without considering the computational cost, whereas the MoP can guarantee the conservation with a bin of finite-sized area.

**TABLE II.** Mass flow rates $\dot{m}_L$, $\dot{m}_R$, and $\dot{m}_B$, respectively, on the left, right, and bottom faces of the control volume (CV) and the time derivative of the mass $\dot{M}_{CV}$ in the CV shown in magenta in the middle panel of Fig. 4.

| Property[a] | MoP | VA |
|---|---|---|
| $\dot{m}_L$ | 4.3 ± 1.8 | 6.0 ± 1.8 |
| $\dot{m}_R$ | 5.5 ± 0.3 | 5.5 ± 0.2 |
| $\dot{m}_B$ | 0.8 ± 0.2 | 0.8 ± 0.2 |
| $\dot{m}_R - \dot{m}_L - \dot{m}_B$[b] | 0.5 ± 1.9 | −1.3 ± 1.8 |
| $-\dot{M}_{CV}$ | ⋯ | 0.5 ± 1.8 |

[a] Defined by Eqs. (18)–(21), all in units of $\times 10^{-7}$ kg/m s.
[b] Mass flux on the top face at the fluid–solid interface is zero.

Indeed, apparent flow features as shown in Fig. 4 can be qualitatively visualized by other methods such as atomic stress,[31] as shown in Appendix C, but the present method provides the distributions of physical properties defined on a surface establishing a direct link with the conservation laws for the arbitrary CV, as shown in Table II, and is generally applicable to a wide range of nanoscale systems with a liquid flow. One of our future research targets is dynamic wetting,[3,4,49] for which we plan to examine the mechanical balance exerted on the fluid around a CV set around the moving contact line as in Fig. 4. Through the comparison with the static case,[17] this would enable the analysis of advancing and receding contact angle from a mechanical point of view.

## IV. CONCLUDING REMARKS

In this work, we developed a calculation method of local stress tensor applicable to non-equilibrium molecular dynamics (NEMD) systems, which evaluates the macroscopic momentum advection and the kinetic term of the stress in the framework of the Method-of-Plane (MoP), in a consistent way to guarantee the mass and the momentum conservation. From the relation between the macroscopic velocity distribution function and the microscopic molecular passage across a fixed control plane, we derived a basic equation to connect the macroscopic field variable and the microscopic molecular variable. Based on the connection, we derived a method to calculate the basic properties of the macroscopic momentum conservation law including the density, velocity, and momentum fluxes as well as the interaction and kinetic terms of the stress tensor defined on a surface with a finite area. Any component of the streaming velocity can be obtained on a control surface, which enables the separation of the kinetic momentum flux into the advection and stress terms in the framework of the MoP, and this guarantees the mass and momentum conservation strictly satisfied for an arbitrary closed control volume (CV) set in NEMD systems. The present MoP method was validated through the extraction of the density and velocity distributions in a quasi-1D steady-state Couette flow system, seeing that the stress tensor distribution by the MoP satisfies the solution of a laminar Couette flow in the bulk, indicating that the flow effect, i.e., the advection term, was removed to evaluate stress properly. Furthermore, we showed the density, velocity, and stress tensor distributions by the MoP even in a quasi-2D system with a moving contact line. We showed that with the present MoP, in contrast to the volume average method, the conservation law was satisfied even for a CV set around the moving contact line, which was located in a strongly inhomegeneous region.

## ACKNOWLEDGMENTS

H.K., T.O., and Y.Y. were supported by the JSPS KAKENHI grant (Nos. JP20J20251, JP18K03929, and JP18K03978), Japan, respectively. Y.Y. was also supported by the JST CREST grant (No. JPMJCR18I1), Japan.

## AUTHOR DECLARATIONS

### Conflict of Interest

The authors have no conflicts to disclose.

## DATA AVAILABILITY

The data that support the findings of this study are available from the corresponding author upon reasonable request.

## APPENDIX A: MACROSCOPIC CONSERVATION LAWS

The macroscopic equation of continuity given with the density $\rho(\boldsymbol{x},t)$ and velocity vector $\boldsymbol{u}(\boldsymbol{x},t)$ both as functions of position $\boldsymbol{x}$ and time $t$ writes

$$\iiint_V \mathrm{d}V \frac{\partial \rho}{\partial t} = -\iint_S \mathrm{d}S \rho u_k n_k, \tag{A1}$$

satisfied for an arbitrary volume $V$ in an enclosing surface $S$, where $n_k$ is the $k$ direction component of the outward unit normal vector $\boldsymbol{n}$ with respect to the infinitesimal surface element d$S$. The Einstein notation is used with a dummy index $k$ for the vectors. Similarly, the macroscopic momentum equation, the Navier–Stokes equation for an arbitrary volume $V$ enclosed by $S$ writes

$$\iiint_V \mathrm{d}V \frac{\partial \rho u_l}{\partial t} = -\iint_S \mathrm{d}S \rho u_l u_k n_k + \iint_S \mathrm{d}S \tau_{kl} n_k + \iiint_V \mathrm{d}V \rho F_l, \tag{A2}$$

where the fluid stress tensor component $\tau_{kl}$ expresses the stress in the $l$ direction exerted on a surface element with an outward normal in the $k$ direction and $F_l$ denotes the external force per mass. Equation (A2) means that the total momentum in $V$ in the LHS can be changed by the momentum flux passing the surface $S$ as well as the impulse due to the stress exerted on the surface $S$, with $\rho$, $\boldsymbol{u}$, and $\tau_{kl}$ defined on $S$, and the external force exerted on the volume $V$, which corresponds to the first, second, and third terms in the RHS, respectively. Specifically, note that the advection $\rho u_l u_k$ and stress $\tau_{kl}$ in the first and second terms of the RHS, respectively, are separated.

## APPENDIX B: INTERACTION TERM FOR TWO-BODY POTENTIAL IN THE MoP

The intermolecular interaction term $\tau_{kl}^{\mathrm{int}}$ in Eq. (1) in the case of a simple two-body potential is calculated by

$$\tau_{kl}^{\mathrm{int}} = -\frac{1}{S_k}\left\langle \sum_{(i,j)\in\mathrm{fluid}}^{\mathrm{across}\ S_k} F_l^{ij} \frac{r_k^{ij}}{|r_k^{ij}|} \right\rangle, \tag{B1}$$

where $r_k^{ij}$ and $F_l^{ij}$ denote the $k$-component of the relative position vector $\boldsymbol{r}^{ij} \equiv \boldsymbol{x}^j - \boldsymbol{x}^i$ and the $l$-component of the force vector $\boldsymbol{F}^{ij}$ on particle $j$ at position $\boldsymbol{x}^j$ from particle $i$ at position $\boldsymbol{x}^i$, respectively. The summation $\sum_{(i,j)\in\mathrm{fluid}}^{\mathrm{across}\ S_k}$ is taken for all line segments of the interparticle interaction between $\boldsymbol{x}^i$ and $\boldsymbol{x}^j$, which cross $S_k$ based on the definition of the IK contour with the straight line connecting each particle pair.[6,26] A sign function $\frac{r_k^{ij}}{|r_k^{ij}|}$ is multiplied for this interaction term to evaluate the force effect depending on the force direction.

## APPENDIX C: STRESS DISTRIBUTION CALCULATED BY THE ATOMIC STRESS

In this section, we compare the stress distribution obtained by the atomic stress with that calculated by the present MoP method.

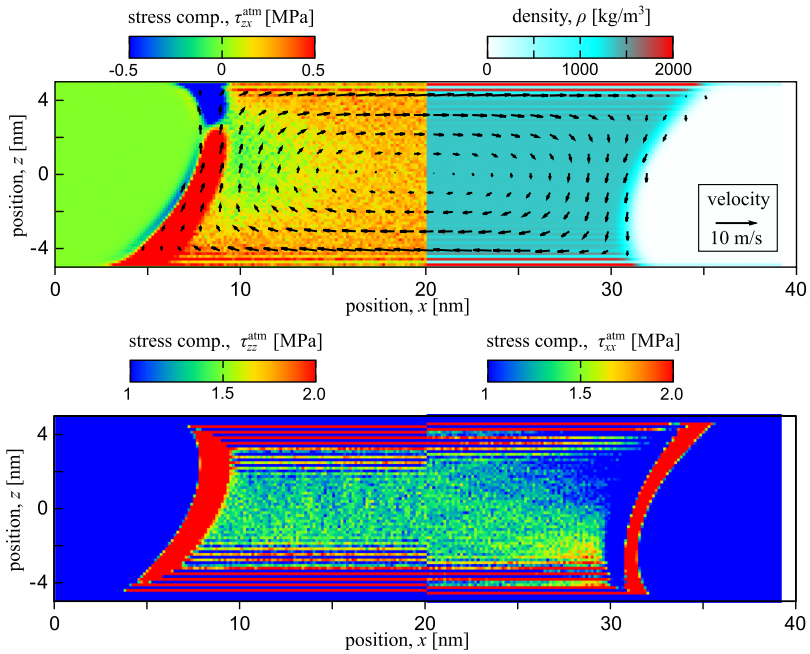


**FIG. 6.** (Top) Distributions of density $\rho$ and velocity $\boldsymbol{u}$ calculated by the VA and off-diagonal volume averaged atomic stress component $\tau_{zx}^{atm}$. The black arrow denotes the macroscopic velocity calculated by the VA. (Bottom) Distributions of the diagonal volume averaged atomic stress components $\tau_{xx}^{atm}$ and $\tau_{zz}^{atm}$.

Atomic stress for mono-atomic molecules interacting with a pair potential is defined as a pointwise stress tensor per atom given by

$$T_{kl}^i = -m(v_k^i - u_k^i)(v_l^i - u_l^i) - \frac{1}{2}\sum_{j\neq i} F_l^{ij} r_k^{ij}, \tag{C1}$$

where $T_{kl}^i$ is the atomic stress tensor of particle $i$, the first and second terms on the RHS are the kinetic and interaction terms, respectively, and $u_k^i$ and $u_l^i$ denote the macroscopic velocity components at the point of the particle. Note that the interaction term is equally allocated to the pair of pointwise atoms $i$ and $j$ in Eq. (C1), in contrast to the MoP that allocates the interaction force on the bin faces through which the interaction force segment between $i$ and $j$ passes.

Figure 6 shows the time-averaged density, velocity, and the stress distributions calculated by volume averaging. The stress $\tau_{kl}^{atm}$ was obtained as the average of the atomic stress $T_{kl}^i$ divided by the local bin volume of $\delta V$, where the averaged velocity of the local volume was used as the macroscopic velocity $\boldsymbol{u}^i$ in Eq. (C1). The size of the bins is the same as that for the MoP and VA. No clear difference was observed between Figs. 4 and 6 in the density and velocity distributions, whereas layered structures appeared only in the distribution of $\tau_{zz}^{atm}$. This unphysical feature is caused by the pointwise approximation of the atomic stress in Eq. (C1).

## REFERENCES

[1]T. Qian, X. P. Wang, and P. Sheng, "Molecular scale contact line hydrodynamics of immiscible flows," Phys. Rev. E **68**, 016306 (2003); arXiv:0210534 [cond-mat].
[2]T. Qian, X. P. Wang, and P. Scheng,"Molecular hydrodynamics of the moving contact line in two-phase immiscible flows," Commun. Comput. Phys. **1**, 1–52 (2006).
[3]T. Omori, Y. Kobayashi, Y. Yamaguchi, and T. Kajishima, "Understanding the asymmetry between advancing and receding microscopic contact angles," Soft Matter **15**, 3923–3928 (2019).
[4]J. Thalakkttor and K. Mohseni, "Role of the rate of surface dilatation in determining microscopic dynamic contact angle," Phys. Fluids **32**, 012111 (2020).
[5]U. Lācis, P. Johansson, T. Fullana, B. Hess, G. Amberg, S. Bagheri, and S. Zaleski, "Steady moving contact line of water over a no-slip substrate," Eur. Phys. J.: Spec. Top. **229**, 1897–1921 (2020).
[6]J. H. Irving and J. G. Kirkwood, "The statistical mechanical theory of transport processes. IV. The equations of hydrodynamics," J. Chem. Phys. **18**, 817–829 (1950).
[7]B. J. Alder and T. E. Wainwright, "Phase transition for a hard sphere system," J. Chem. Phys. **27**, 1208–1209 (1957).
[8]B. J. Alder and T. E. Wainwright, "Studies in molecular dynamics. I. General method," J. Chem. Phys. **31**, 459–466 (1959).
[9]D. Evans and G. Morriss, *Statistical Mechanics of Nonequilibrium Liquids*, 2nd ed. (Cambridge University Press, 2008), pp. 71–72.
[10]M. P. Allen and D. J. Tildesley, *Computer Simulation of Liquids*, 2nd ed. (Oxford University Press, 2017).
[11]D. H. Tsai, "The virial theorem and stress calculation in molecular dynamics," J. Chem. Phys. **70**, 1375–1382 (1979).
[12]S. M. Thompson, K. E. Gubbins, J. P. R. B. Walton, R. A. R. Chantry, and J. S. Rowlinson, "A molecular dynamics study of liquid drops," J. Chem. Phys. **81**, 530–542 (1984).
[13]B. D. Todd, D. J. Evans, and P. J. Daivis, "Pressure tensor for inhomogeneous fluids," Phys. Rev. E **52**, 1627–1638 (1995).
[14]M. Han and J. S. Lee, "Method for calculating the heat and momentum fluxes of inhomogeneous fluids," Phys. Rev. E **70**, 061205 (2004).
[15]B. D. Todd and P. J. Daivis, *Nonequilibrium Molecular Dynamics: Theory, Algorithms and Applications* (Cambridge University Press, 2017).
[16]R. J. Hardy, "Formulas for determining local properties in molecular-dynamics simulations: Shock waves," J. Chem. Phys. **76**, 622–628 (1982).
[17]Y. Yamaguchi, H. Kusudo, D. Surblys, T. Omori, and G. Kikugawa, "Interpretation of Young's equation for a liquid droplet on a flat and smooth solid surface: Mechanical and thermodynamic routes with a simple Lennard-Jones liquid," J. Chem. Phys. **150**, 044701 (2019).
[18]J. F. Lutsko, "Stress and elastic constants in anisotropic solids: Molecular dynamics techniques," J. Appl. Phys. **64**, 1152–1154 (1988).

[19]J.-G. Weng, S. Park, J. R. Lukes, and C.-L. Tien, "Molecular dynamics investigation of thickness effect on liquid films," J. Chem. Phys. **113**, 5917–5923 (2000).
[20]J. Cormier, J. M. Rickman, and T. J. Delph, "Stress calculation in atomistic simulations of perfect and imperfect solids," J. Appl. Phys. **89**, 99–104 (2001).
[21]D. M. Heyes, E. R. Smith, D. Dini, and T. A. Zaki, "The equivalence between volume averaging and method of planes definitions of the pressure tensor at a plane," J. Chem. Phys. **135**, 024512 (2011).
[22]J. Z. Yang, X. Wu, and X. Li, "A generalized Irving–Kirkwood formula for the calculation of stress in molecular dynamics models," J. Chem. Phys. **137**, 134104 (2012).
[23]D. M. Heyes, D. Dini, and E. R. Smith, "Equilibrium fluctuations of liquid state static properties in a subvolume by molecular dynamics," J. Chem. Phys. **145**, 104504 (2016).
[24]E. R. Smith, D. M. Heyes, and D. Dini, "Towards the Irving–Kirkwood limit of the mechanical stress tensor," J. Chem. Phys. **146**, 224109 (2017).
[25]E. R. Smith and C. Braga, "Hydrodynamics across a fluctuating interface," J. Chem. Phys. **153**, 134705 (2020).
[26]K. Shi, E. E. Santiso, and K. E. Gubbins, "Can we define a unique microscopic pressure in inhomogeneous fluids?," J. Chem. Phys. **154**, 084502 (2021).
[27]G. Bakker, *Kapillarität und Oberflächenspannung* (Wien-Harms, 1928), Vol. 6.
[28]J. S. Rowlinson and B. Widom, *Molecular Theory of Capillarity* (Dover, 1982).
[29]S. Nishida, D. Surblys, Y. Yamaguchi, K. Kuroda, M. Kagawa, T. Nakajima, and H. Fujimura, "Molecular dynamics analysis of multiphase interfaces based on in situ extraction of the pressure distribution of a liquid droplet on a solid surface," J. Chem. Phys. **140**, 074707 (2014).
[30]D. Surblys, Y. Yamaguchi, K. Kuroda, M. Kagawa, T. Nakajima, and H. Fujimura, "Molecular dynamics analysis on wetting and interfacial properties of water-alcohol mixture droplets on a solid surface," J. Chem. Phys. **140**, 034505 (2014).
[31]A. P. Thompson, S. J. Plimpton, and W. Mattson, "General formulation of pressure and stress tensor for arbitrary many-body interaction potentials under periodic boundary conditions," J. Chem. Phys. **131**, 154107 (2009).
[32]S. Plimpton, "Fast parallel algorithms for short-range molecular dynamics," J. Comput. Phys. **117**, 1–19 (1995).
[33]D. Surblys, H. Matsubara, G. Kikugawa, and T. Ohara, "Application of atomic stress to compute heat flux via molecular dynamics for systems with many-body interactions," Phys. Rev. E **99**, 051301 (2019).
[34]A. Harashima, "Statistical mechanics of surface tension," J. Phys. Soc. Jpn. **8**, 343–347 (1953).
[35]A. Harashima, *Molecular Theory of Surface Tension*, Advances in Chemical Physics Vol. 1 (Wiley, 1958), p. 203.
[36]D. Schofield and J. R. Henderson, "Statistical mechanics of inhomogeneous fluids," Proc. R. Soc. London, Ser. A **379**, 231–246 (1982).
[37]J. S. Rowlinson, "Thermodynamics of inhomogeneous systems," Pure Appl. Chem. **65**, 873–882 (1993).
[38]B. Hafskjold and T. Ikeshoji, "Microscopic pressure tensor for hard-sphere fluids," Phys. Rev. E **66**, 011203 (2002).
[39]K. Shi, Y. Shen, E. E. Santiso, and K. E. Gubbins, "Microscopic pressure tensor in cylindrical geometry: Pressure of water in a carbon nanotube," J. Chem. Theory Comput. **16**, 5548–5561 (2020).
[40]H. Kusudo, T. Omori, and Y. Yamaguchi, "Extraction of the equilibrium pinning force on a contact line exerted from a wettability boundary of a solid surface through the connection between mechanical and thermodynamic routes," J. Chem. Phys. **151**, 154501 (2019).
[41]Y. Imaizumi, T. Omori, H. Kusudo, C. Bistafa, and Y. Yamaguchi, "Wilhelmy equation revisited: A lightweight method to measure liquid-vapor, solid-liquid, and solid-vapor interfacial tensions from a single molecular dynamics simulation," J. Chem. Phys. **153**, 034701 (2020).
[42]H. C. Andersen, "Rattle: A 'velocity' version of the shake algorithm for molecular dynamics calculations," J. Comput. Phys. **52**, 24–34 (1983).
[43]P. J. Daivis, K. P. Travis, and B. D. Todd, "A technique for the calculation of mass, energy, and momentum densities at planes in molecular dynamics simulations," J. Chem. Phys. **104**, 9651–9653 (1996).
[44]K. Ogawa, H. Oga, H. Kusudo, Y. Yamaguchi, T. Omori, S. Merabia, and L. Joly, "Large effect of lateral box size in molecular dynamics simulations of liquid-solid friction," Phys. Rev. E **100**, 023101 (2019).
[45]H. Oga, Y. Yamaguchi, T. Omori, S. Merabia, and L. Joly, "Green-Kubo measurement of liquid-solid friction in finite-size systems," J. Chem. Phys. **151**, 054502 (2019).
[46]J. Blömer and A. E. Beylich, "Molecular dynamics simulation of energy accommodation of internal and translational degrees of freedom at gas-surface interfaces," Surf. Sci. **423**, 127–133 (1999).
[47]C. Bistafa, D. Surblys, H. Kusudo, and Y. Yamaguchi, "Water on hydroxylated silica surfaces: Work of adhesion, interfacial entropy, and droplet wetting," J. Chem. Phys. **155**, 064703 (2021).
[48]J.-C. Fernández-Toledano, T. D. Blake, , and J. De Coninck, "Contact-line fluctuations and dynamic wetting," J. Colloid Interface Sci. **540**, 322–329 (2019).
[49]Y. Hizumi, T. Omori, Y. Yamaguchi, and T. Kajishima, "Study on the Navier boundary condition for flows with a moving contact line by means of molecular dynamics simulation," Trans. JSME **81**, 15-00409 (2015) (in Japanese).